A Computational Study of the Hydroxy-Group Directivity in the Peroxyformic Acid Epoxidation of the Chiral Allylic Alcohol (*Z*)-3-Methyl-3-penten-2-ol: Control of Threo Diastereoselectivity through Allylic Strain and Hydrogen Bonding

Waldemar Adam,*[,†] Robert D. Bach,*[,‡] Olga Dmitrenko,[‡] and Chantu R. Saha-Möller[†]

Institute of Organic Chemistry, University of Würzburg, Am Hubland, D-97074 Würzburg, Germany, and Department of Chemistry and Biochemistry, University of Delaware, Newark, Delaware19716

rbach@udel.edu

Received June 23, 2000

Eight transition structures for the epoxidation of the chiral allylic alcohol (*Z*)-3-methyl-3-penten-2-ol (**1**) with peroxyformic acid have been computed by the B3LYP density functional method with 6-31G(d) and 6-31G(d,p) basis sets. The four lowest-energy transition structures and their respective pre-reaction clusters were fully re-optimized by employing 6-311+G(d,p) and correlation-consistent polarized valence triple-ζ cc-pZTV basis sets. The relative energies of the transition structures were found to be highly sensitive to the basis set applied. The transition state for threo product formation, *anti*-(2*S*,3*R*,4*S*)-TS-**3f**, with the lowest total energy (at B3LYP/611+G(d,p) and B3LYP/AUG-cc-pZTV) of all the TSs examined, has a planar peracid moiety and is a precursor for the 1,4 migration of the peracid hydrogen atom H_a to the peroxy oxygen atom O_4. The use of different basis sets does not affect markedly the geometry of the *anti*-(2*S*,3*R*,4*S*)-TS-**3f** transition structure. The transition state for erythro epoxidation, *syn*-(2*R*,3*R*,4*S*)-TS-**3a**, is 0.9 kcal/mol higher in energy and possesses a nonplanar peracid approaching the C=C bond in a manner intermediate between spiro and planar. The relative energy and nonplanarity of this syn transition structure is highly sensitive to the basis set applied. With the smaller basis set, 6-31G(d,p), it is actually the lowest-energy TS and the peracid moiety is significantly skewed. The contribution of the four lowest energy transition stuctures **3a**, **3b**, **3e**, and **3f** to the threo/erythro product ratio has been assessed through an extended Curtin−Hammet principle analysis of this multi-transition state reaction. It has been found that this approach agrees well with the experimental threo/erythro product ratio, in particular when the corrections for a solvent effect are made within the self-consistent isodensity polarized continuum model (SCI-PCM).

Introduction

Stereochemical control of the peracid epoxidation of olefins has been a subject of intense interest since the discovery of this reaction by Prileschajew in 1909.[1] In 1950, the mechanistic details of the oxygen transfer were described by Bartlett[2] in terms of the ground-breaking planar "butterfly" transition state. The pioneering studies by Henbest[3] in 1957 mark the first demonstration that the stereochemical course of the Prileschajew epoxidation may be steered through synergistic interplay between conformational and hydrogen-bonding effects in chiral allylic alcohols, a mechanistic concept which we have designated as *hydroxy-group directivity*.[4] For 3-hydroxycyclohexene it was shown[3] that the cis epoxide was favored, which signifies that the perbenzoic acid attacks the π bond from the same side that bears the allylic alcohol functionality. That hydrogen bonding between the peracid and allylic alcohol substrate is responsible for the observed syn epoxidation (substrate control[5]) was confirmed by the fact that on masking the hydroxy group in the form of methyl or acetyl derivatives, i.e., 3-methoxy- and 3-acetoxycyclohexene, then predominantly the trans epoxides were produced.[3] The preferred anti attack of the peracid was rationalized in terms of steric effects since hydrogen bonding by the allylic substitutents with the peracid cannot apply.

Acyclic allylic alcohols lack the inherent advantages of cyclic ones in regard to conformational preferences, unless imposed through appropriate substitution. The concept of allylic strain serves this purpose,[6] which allows differentiation of the two π faces of the olefinic double bond by adequate alignment of the hydroxy group through steric effects. This is conveniently illustrated for the chiral allylic alcohol (*Z*)-3-methyl-3-penten-2-ol (**1**), which we have introduced as a stereochemical probe to assess transition structures in oxygen-transfer reactions (Scheme 1). In this substrate, both 1,3-allylic ($A^{1,3}$, i.e., steric repulsion between the C_1 and C_5 methyl groups) and 1,2-allylic ($A^{1,2}$, i.e., steric repulsion between the C_1

* To whom correspondence should be addressed. (W.A.) Fax: + 49 (931) 888 4756. E-mail: adam@chemie.uni-wuerzburg.de. wwwhttp://www.organik.uni-wuerzburg.de. (R.D.B.) Fax: +1(302) 831 6335. wwwhtttp: www.udel.edu/chem/bach.

† University of Würzburg.

‡ University of Delaware.

(1) Prileschajew, N. *Ber.* **1909**, *42*, 4811−4815.

(2) Bartlett, P. D. *Rec. Chem. Prog.* **1950**, *11*, 47−51.

(3) (a) Henbest, H. B.; Wilson, R. A. L. *J. Chem. Soc.* **1957**, 1958−1965. (b) Henbest, H. B. *Proc. Chem. Soc.* **1963**, 159−165.

(4) Adam, W.; Wirth, T. *Acc. Chem. Res.* **1999**, *32*, 703−710.

(5) For an excellent review on substrate-directed chemical reactions see: Hoveyda, A. H.; Evans, D. A.; Fu, G. C. *Chem. Rev.* **1993**, *93*, 1307−1370.

(6) Hoffmann, R. W. *Chem. Rev.* **1989**, *89*, 1841−1860.

10.1021/jo0009548 CCC: $19.00
Published on Web 09/13/2000

Scheme 1

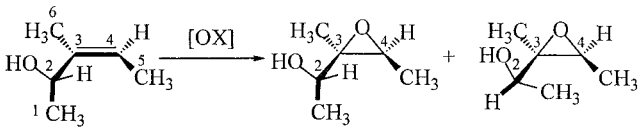

1 *2S,3R,4S* *threo (2S,3R)* *2R,3R,4S* *erythro (2R,3R)*

m-CPBA	90	:	10
$VO(acac)_2$ / *t*-BuOOH	33	:	67

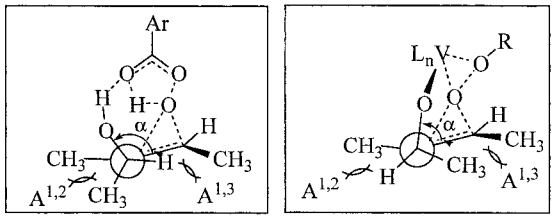

α ca. 120∞ $40∞ < α < 50∞$

and C_6 methyl groups) strain are in competition. This gauges the $C_4-C_3-C_2-O_1$ dihedral angle about the olefinic plane and thereby aligns the hydroxy group in a favored conformation for hydrogen bonding with the approaching oxidant. This *hydroxy group directivity* manifests itself experimentally in terms of the threo/erythro diastereomeric ratio (dr) that is observed for the resulting epoxides (Scheme 1).

Two oxidants shall serve as extreme cases to demonstrate the importance of the $C_4-C_3-C_2-O_1$ dihedral angle (α) for controlling the stereochemical course in the epoxidation of the allylic alcohol **1**. These are *m*-chloroperbenzoic acid (*m*-CPBA) and $VO(acac)_2$/*t*-BuOOH, for which the dr values are given in Scheme 1.[7] The stereochemical differences are evident in that the epoxidation of **1** by *m*-CPBA is threo-selective, while $VO(acac)_2$/*t*-BuOOH gives predominantly the erythro product. The transition structures in Scheme 1 disclose what is mechanistically going on to rationalize this stereochemical dichotomy. The dihedral angles (α) have been empirically estimated at ca. 120° for the *m*-CPBA transition state and between 40° and 50° for $VO(acac)_2$/*t*-BuOOH, but for allylic alcohols without allylic strain.[8] The obtuse (α ca. 120°) dihedral angle in the case of *m*-CPBA is favorable for substrate−oxidant hydrogen bonding and results in threo diastereoselectivity, which is conditioned by minimal 1,3-allylic strain. In contrast, the acute (40° < α < 50°) dihedral angle for $VO(acac)_2$/*t*-BuOOH derives from metal−alcoholate bonding and erythro diastereoselectivity is favored, imposed by minimal 1,2-allylic strain.

Clearly, the chiral allylic alcohol **1** constitutes a useful stereochemical probe to assess transition structures and herewith provides valuable mechanistic information on oxygen-transfer processes. However, the structural details of the transition-state geometries have been inferred from ground-state conformations of the allylic substrate **1** and not directly from the transition states for the peracid epoxidation. The latter requires computational methodology, the purpose of the present study, to scrutinize whether the above chemical intuition is reliable. In this regard, the epoxidation of allyl alcohol (the parent allylic alcohol, 2-propen-1-ol), by peroxyformic acid has been investigated computationally and the importance of hydrogen bonding between the allylic hydroxy group and peracid carbonyl functionality established.[9a] More recently, the peroxy oxygen atoms of the peracid have also been identified as hydrogen-bond acceptors in the transition state for the epoxidation of allyl alcohol.[10]

Thus, hydrogen bonding to either the carbonyl (O_4) or the peroxy oxygen (O_2) atoms serves to direct the peracid to the C=C π face that bears the hydroxy group of allyl alcohol with nearly equal proficiency (see $\mathbf{TS_{AA}}$, Figure 1). Although much valuable insight into the details of the hydrogen bonding in directing the peracid attack on allyl alcohol itself has been garnered, unfortunately, this achiral substrate does not possess stereochemical information to cross-check with experimental diastereoselectivities. In this regard, the reaction coordinate for the peroxyformic acid epoxidation of the chiral allylic alcohol **1** was computed according to density functional theory to evaluate the mechanistic concept of *hydroxy-group directivity* in terms of allylic strain and hydrogen bonding and rationalize the observed threo diastereoselectivity. We specifically address the role of hydrogen bonding in the syn versus anti approach of the peracid onto the allylic hydroxyl directing group on the activation barrier for epoxidation.

Computational Methods

Ab initio molecular orbital calculations were performed with the GAUSSIAN 94 and GAUSSIAN 98 system of programs.[11] The Becke three-parameter hybrid functional[12a,13a] combined with the Lee, Yang, and Parr (LYP) correlation functional,[12b] denoted B3LYP,[13b] was employed in the calculations using

(7) (a) Adam, W.; Nestler, B. *J. Am. Chem. Soc.* **1992**, *114*, 6549−6550. (b) Adam, W.; Nestler, B. *J. Am. Chem. Soc.* **1993**, *34*, 5041−5049. (c) Adam, W.; Nestler B. *Tetrahedron Lett.* **1993**, *34*, 611−614.

(8) (a) Rossiter, B. E.; Verhoeven, T. R.; Sharpless, K. B. *Tetrahedron Lett.* **1979**, *20*, 4733−4736. (b) Sharpless, K. B.; Verhoeven, T. R. *Aldrichim. Acta* **1979**, *12*, 63−73.

(9) (a) Bach, R. D.; Estévez, C. M.; Winter, J. E.; Glukhoutsev, M. N. *J. Am. Chem. Soc.* **1998**, *120*, 680−685. (b) Bach, R. D.; Glukhovtsev, M. N.; Gonzalez, C. *J. Am. Chem. Soc.* **1998**, *120*, 9902−9910. (c) Bach, R. D.; Winter, J. E.; McDouall, J *J. Am. Chem. Soc.* **1995,** *117*, 8586. (d) Bach, R. D.; Ayala, P. Y.; Schlegel, H. B. *J. Am. Chem. Soc.* **1996**, *118*, 12758−12765.

(10) (a) Freccero, M.; Gandolfi, R.; Sarzi-Amadè, M.; Rastelli, A. *J. Org. Chem.* **1999**, *64*, 3853−3860. (b) Freccero, M.; Gandolfi, R.; Sarzi-Amadè, M.; Rastelli, A. *J. Org. Chem.* **2000**, *65*, 2030−2042.

(11) (a) Theoretical calculations were carried out by using the Gaussian 94 and Gaussian 98 program system (ref 11b,c) with gradient geometry optimization. (b) Frisch, M. J.; Trucks, G. W.; Schlegel, H. B.; Scuseria, G. E.; Robb, M. A.; Cheeseman, J. R.; Zakrzewski, V. G.; Montgomery, J. A.; Stratmann, R. E.; Burant, J. C.; Dapprich, S.; Millam, J. M.; Daniels, A. D.; Kudin, K. N.; Strain, M. C.; Farkas, O.; Tomasi, J.; Barone, V.; Cossi, M.; Cammi, R.; Mennucci, B.; Pomelli, C.; Adamo, C.; Clifford, S.; Ochterski, J.; Petersson, G. A.; Ayala, P. Y.; Cui, Q.; Morokuma, K.; Malick, D. K.; Rabuck, A. D.; Raghavachari, K.; Foresman, J. B.; Cioslowski, J.; Ortiz, J. V.; Baboul, A. G.; Stefanov, B. B.; Liu, G.; Liashenko, A.; Piskorz, P.; Komaromi, I.; Gomperts, R.; Martin, R. L.; Fox, D. J.; Keith, T.; Al-Laham, M. A.; Peng, C. Y.; Nanayakkara, A.; Gonzalez, C.; Challacombe, M.; Gill, P. M. W.; Johnson, B.; Chen, W.; Wong, M. W.; Andres, J. L.; Gonzalez, C.; Head-Gordon, M.; Replogle, E. S.; Pople, J. A. Gaussian 98, Revision A.7, Gaussian, Inc., Pittsburgh, PA, 1998. (c) González, C.; Schlegel, H. B. *J. Chem. Phys.* **1989**, *90*, 2154−2161. (d) Gonzalez, C.; Schlegel, H. B. *J. Phys. Chem.* **1990**, *94*, 5523−5327.

(12) (a) Becke, A. D. *Phys. Rev. A* **1988**, 38, 3098−3100. (b) Lee, C.; Yang, W.; Parr, R. G. *Phys. Rev. B* **1988**, *37*, 785−789.

(13) (a) Becke, A. D. *J. Chem. Phys.* **1993**, *98*, 5648−5652. (b) Stephens, P. J.; Devlin, F. J.; Chabalowski, C. F.; Frisch, M. J. *J. Phys. Chem.* **1994**, *98*, 11623−11627.

density functional theory (DFT). Geometries were optimized[14] initially with the 6-31G(d) and 6-31G(d,p) basis sets and then with the 6-311+G(d,p), cc-pVTZ and AUG-cc-pVTZ basis sets.[11,15] The cc-pVTZ, Dunning's triple ς correlation consistent basis set includes polarization functions 2s,2p,1d for H and He, 4s,2p,2d,1f for B−Ne and 5s,4p,2d,1f for Al−Ar (526 basis functions in the present system).[15a,b] Geometry optimizations of the four lowest-energy TSs with the AUG-cc-pVTZ basis set (augmented with p functions on hydrogen and f functions on the heavy atoms) required 828 basis functions.

The stationary points on the potential energy surfaces were characterized by calculations of vibrational frequencies at the B3LYP/6-31G* level. Zero-point energies (ZPE), computed at the B3LYP/6-31G(d) level, were scaled by 0.9804.[16]

Solvent effects have been studied in terms of the PCM[17a] and SCIPCM[17b] models with B3LYP/6-31G(d) and B3LYP/6-311+G(d,p) basis sets. A dielectric constant $\epsilon = 8.9$ was used to model methylene chloride. Throughout the text, bond lengths are in angstroms and bondangles are in degrees.

Results and Discussion

All the conformational searches applied in this study (Table S1 in the Supporting Information) on the allylic alcohol **1** disclosed **1a** as the global ground-state mimimum energy conformer. The energy gap between **1a** and **1b** (the next lowest energy conformer, Figure 2) increases with an increase in the size of the basis set. The total energy difference is 0.68 kcal/mol at B3LYP/6-31G(d,p), whereas with the B3LYP/cc-pVTZ basis set, **1a** is 1.19 kcal/mol lower in energy (Figure 2). The differences between these two conformational isomers are evident from the various pertinent dihedral angles given in Figure 2, which express the compromise between $A^{1,2}$ and $A^{1,3}$ strain. As illustrated for the racemic allylic alcohol **1**, in the lowest energy conformer **1a**, the $C_4-C_3-C_2-O_1$ dihedral angle is 119.5° compared to 37.5° for conformer **1b**. Thus, the C_1 methyl group at the C_2 stereogenic center is farthest away from the C_5 methyl group in conformer **1a**, and thereby $A^{1,3}$ strain is minimized. However, $A^{1,2}$ strain is more favorable in the **1b** conformer compared to **1a**, as revealed by the $C_6-C_3-C_2-C_1$ dihedral angles of 94.2° and 60.2° (Figure 2). As is well established,[4] between $A^{1,2}$ and $A^{1,3}$ strain, the latter dominates for peracid oxidations and in the particular case of conformers **1a** and **1b**, the compromise is 1.19 kcal/mol in favor of the former. The other dihedral angles $C_6-C_3-C_2-O_1$ and $C_4-C_3-C_2-C_1$ (Figure 2) substantiate this conformational analysis. As a consequence, the allylic hydroxy group at the C_2 chirality center is oriented toward the *Si* face in both conformers **1a** and **1b**. It is more convenient and easier to follow the stereochemical course of the reaction by allowing the oxidant to attack the allylic alcohol from the same π face (in Figure 2 it is the *Si* face), which obliges that opposite enantiomers of the racemic alcohol, i.e., *2S* for **1a** and *2R* for **1b**, are involved. For the **1a** conformer, the allylic hydroxy group points more perpendicularly to the π bond than for **1b** and, therefore, in principle it is better oriented toward interaction with the incoming oxidant, e.g., through hydrogen bonding. More significantly, since for both enantiomers the hydroxy group points to the same π face, namely the *Si* one, we expect that the hydroxy group should direct the diastereoselectivity of the epoxidation, as is experimentally well documented.[4] Thus, the **1a** conformer will afford the 2*S*,3*R*,4*S* epoxide (threo configuration about the C_2-C_3 bond) and the **1b** conformer the 2*R*,3*R*,4*S* one (erythro configuration about the C_2-C_3 bond).

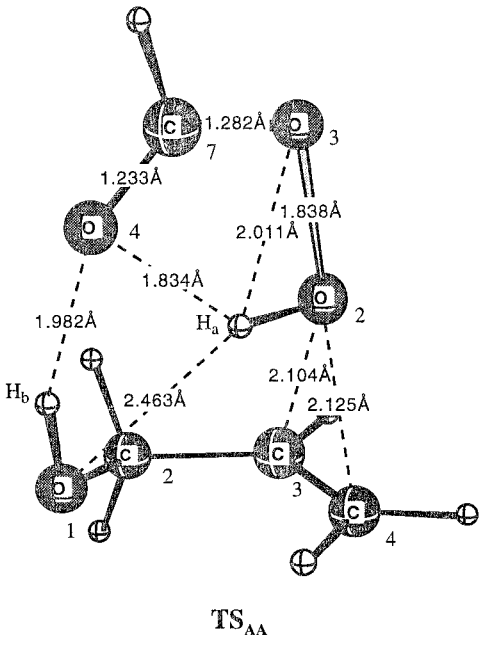

Figure 1. Lowest energy transition structure $\mathbf{TS_{AA}}$ for the epoxidation of allyl alcohol at the B3LYP/6-311G(d,p) level (see ref 9a,**TS-2a** structure)

The hydroxy group directivity is already manifested in the pre-reaction clusters **2a**−**d** (Figure 3), which constitute the hydrogen-bonded conglomerates between the two conformers of allylic alcohol **1** and peroxyformic acid that correspond to the four lowest energy TSs. All the pre-reaction clusters have relatively long distances between the O_2 peroxy oxygen atom and the π bond, but in each case the electrophilic oxygen O_2 is ideally poised to be transferred to the C=C in the TS for epoxidation. The balance between steric interactions and relatively strong hydrogen bonding network renders structure **2b** to be the lowest-energy pre-reaction cluster.

Stereochemical Assignment of the Transition Structures and Analysis of the Relative Energetics of Epoxidation. The next step along the epoxidation reaction coordinate is to locate the minimum energy transition structure for the oxygen-transfer step. Eight structural options (**3a**−**h**, Figures 4 and 5 and Table 1) shall be considered for this complex process: (i) The two conformers **1a** and **1b** (Figure 2) of the allylic alcohol **1**, (ii) the two configurations 2*S* and 2*R* at the stereogenic

(14) (a) Schlegel, H. B. *J. Comput. Chem.* **1982**, *3*, 214−218. (b) Schlegel, H. B. *Adv. Chem. Phys.* **1987**, *67*, 249−286. (c) Schlegel, H. B. In *Modern Electronic Structure Theory*; Yarkony, D. R., Ed.; World Scientific: Singapore, 1995; p 459.

(15) (a) Dunning, T. H., Jr. *J. Chem.* Phys. **1989**, *90*, 1007. (b) Kendall, R. A.; Dunning Jr., T. H.; Harrison, R. J. *J. Chem. Phys.* **1992**, *96*, 6796. (c) Peterson, K. A.; Woon, D. E.; Dunning, T. H., Jr. *J. Chem. Phys.* **1994**, *100*, 7410. (d) Curtis, L. A.; McGrath, M. P.; Blaudeau, J.-P., Davis, N. E.; Binning, R. C., Jr.; Radom, L. *J. Chem. Phys.* **1995**, *103*, 6104.

(16) Wong, M. W. *Chem. Phys. Lett.* **1996**, *256*, 391−399.

(17) (a) Miertus, S.; Tomasi, J. *Chem. Phys.* **1982**, *65*, 239−245. (b) Foresman J. B,; Keith, T. A.; Wiberg K. B.; Snoonian J.; Frisch, M. J *J. Phys. Chem.* **1996**, *100*, 16098−16104.

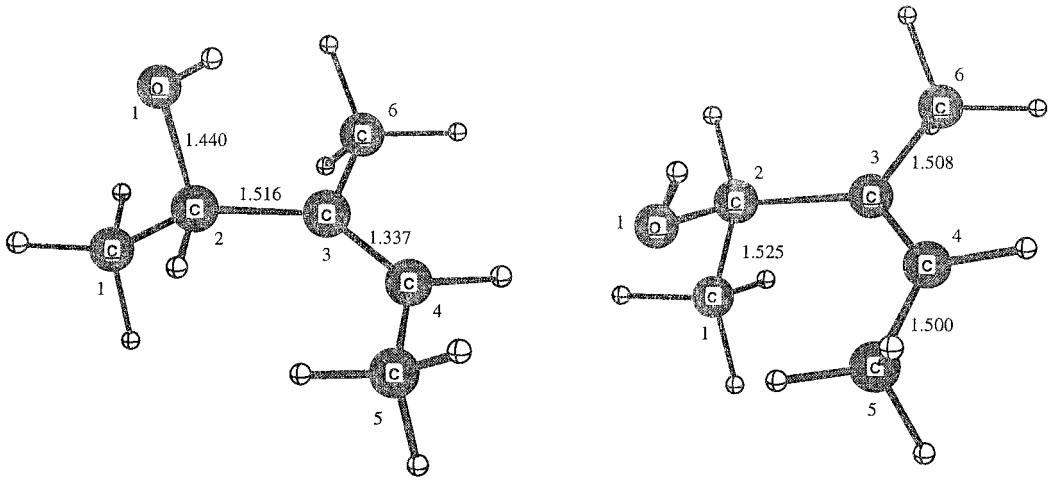

Conformer 1a

E_{tot}=-311.19092 a.u.
E_{rel}=0.00 kcal/mol, μ=1.54 D

C_4-C_3-C_2-O_1 = 119.5
C_4-C_3-C_2-C_1 = -121.0
C_6-C_3-C_2-C_1 = 60.2
C_6-C_3-C_2-O_1 = -59.3

Conformer 1b

E_{tot}=-311.18902 a.u.
E_{rel}=1.19 kcal/mol, μ=1.32 D

C_4-C_3-C_2-O_1 = 37.5
C_4-C_3-C_2-C_1 = -84.4
C_6-C_3-C_2-C_1 = 94.2
C_6-C_3-C_2-O_1 = -143.8

Figure 2. Two primary conformations **1a** and **1b** of the (*Z*)-3-methyl-3-penten-2-ol (**1**) optimized at the B3LYP/cc-pVTZ level of theory. The relative energies (E_{rel}) are based upon total energies.

Table 1. Selected Thermodynamic Parameters (T = 298.15 K) for the Transition Structures 3a−h and Pre-Reaction Clusters 2a−c. All the Relative Data Are Given with Respect to the Isolated Reactants, Peroxyformic Acid, and Lowest Energy Conformer 1a. (For Total Energies, ZPE, and Entropies of Reactants and Transition Structures see Table S1 in the Supporting Information)

	$\Delta E^{\ddagger(a)}$ 6-31G** (kcal/mol)	$\Delta E^{\ddagger\,a}$ 6-311 +G** (kcal/mol)	$\Delta E^{\ddagger\,a}$ cc-pVTZ (kcal/mol)	$\Delta H^{\ddagger\,b}$ 6-311 +G** (kcal/mol)	$\Delta H^{\ddagger\,b}$ cc-pVTZ (kcal/mol)	$\Delta G^{\ddagger\,c}$ 6-311 +G** (kcal/mol)	$\Delta G^{\ddagger\,c}$ cc-pVTZ (kcal/mol)	$\Delta G_{solv}{}^{\ddagger\,d}$ 6-311 +G** (kcal/mol)	$\Delta G_{solv}{}^{\ddagger\,d}$ cc-pVTZ (kcal/mol)	$\Delta S^{\ddagger\,e}$ 6-31G* (eu)
3a	4.88	7.78	9.70	7.91	9.83	20.91	22.82	22.00	23.91	−43.59
3b	6.10	7.81	10.05	7.70	9.95	19.68	21.92	20.54	22.78	−40.17
3c	10.39									−43.32
3d	10.00									−40.87
3e	5.83	7.75	9.46	7.82	9.54	20.30	22.01	21.44	23.15	−41.86
3f	5.62	6.77	9.20	6.70	9.13	18.63	21.06	19.21	21.65	−40.02
3g	6.20	9.37		9.56		22.87		23.97		−44.61
3h	7.81									−40.28
2a	−6.31	−3.9	−4.18	−2.61	−2.83	7.17	6.95	9.33	9.11	−32.82
2b	−8.94	−5.91	−5.76	−4.32	−4.17	5.80	5.95	8.52	8.66	−33.95
2c		−2.33	−2.78	−1.07	−1.15	8.92	8.47	11.55	11.10	−33.50
2d		−4.44	−4.75	−3.76	−4.07	6.79	6.48	9.09	8.78	−35.39

[a] Classical activation barrier computed from the sum of the total energies (E_0) of the isolated reactants by using B3LYP. [b] Activation enthalpy (B3LYP, T = 298 K) with respect to isolated reactants. The thermal correction numbers have been calculated for each structure at B3LYP/6-31G(d) level and scaled by 0.9804. [c] Free energy of activation computed by using B3LYP/6-31G* entropy and thermal corrections. [d] Free energy of activation computed with the solvent correction (B3LYP/6-31G(d), SCIPCM, ϵ = 8.9) taken into account. [e] Activation entropy from the isolated reactants.

center of this substrate, and (iii) the syn and anti approaches of the peroxyformic acid carbonyl group with respect to the allylic hydroxy group in the spiro[9b,18] geometry. In this way, eight transition structures were located initially with the 6-31G(d) basis set and then re-optimized at 6-31G(d,p) (Figure S1 and Table S1 in the Supporting Information).

When the peracid carbonyl group points toward the allylic hydroxy group, as in **3a**, **3c**, **3e**, and **3g**, these transition structures are denoted by the syn descriptor and entail the H_b−O_4 hydrogen bonding to the carbonyl oxygen. When the carbonyl group points away, as in **3b**,

(18) (a) Bach, R. D.; Willis, C. L.; Domagals, J. M. In *Applications of MO Theory in Organic Chemistry*: Csizmadia, I. C., Ed.; Elsevier Scientific: Amsterdam, 1977; Vol. 2, p 221. (b) Bach, R. D.; Andrés, J. L.; Davis, F. A. *J. Org. Chem.* **1992**, *57*, 613−618.

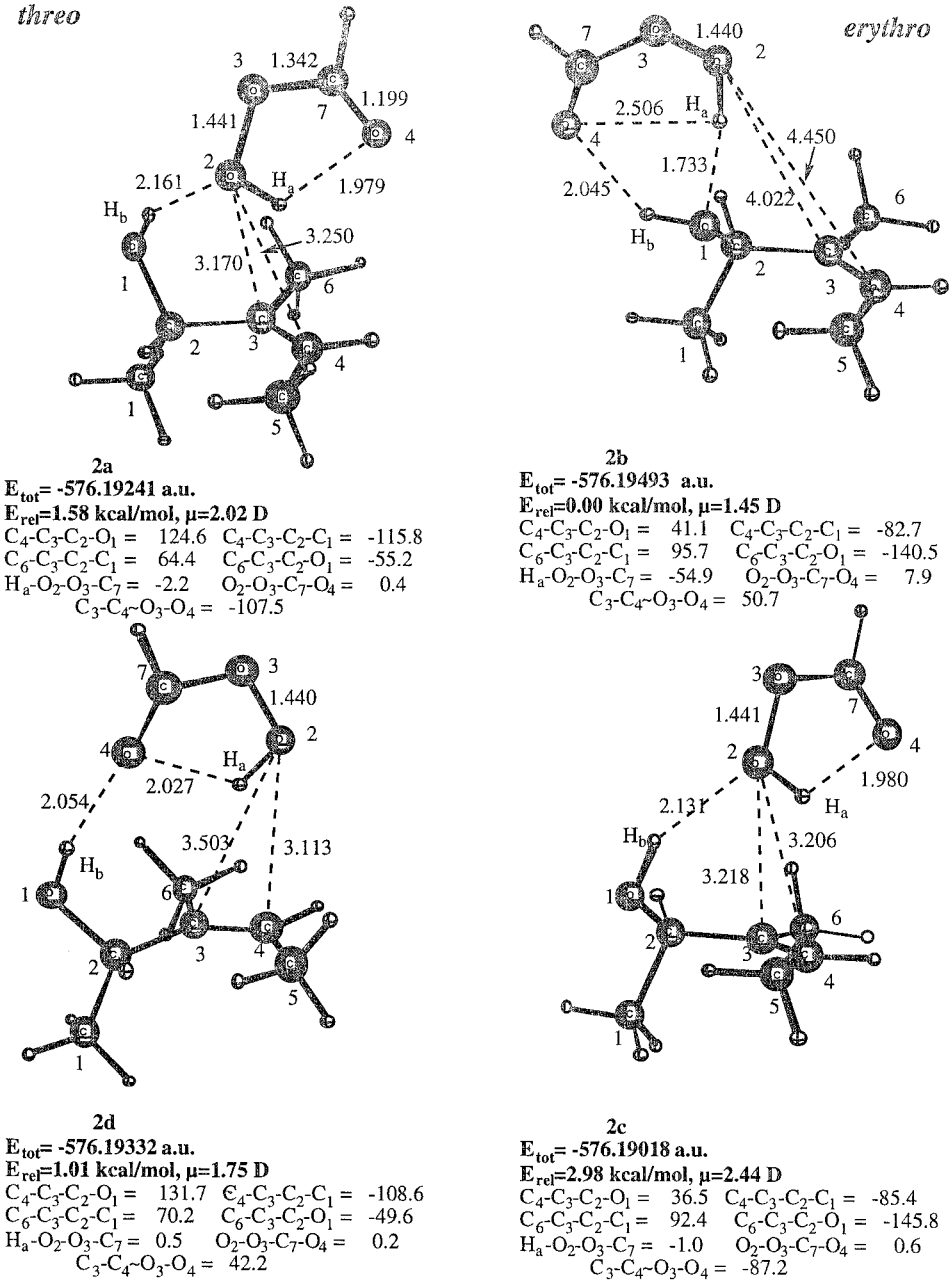

Figure 3. Lowest-energy pre-reaction clusters of peroxyformic acid and (*Z*)-3-methyl-3-penten-2-ol (**1**) optimized at the B3LYP/cc-pVTZ level of theory. The relative energies (E_{rel}) are based upon total energies.

3d, **3f**, and **3h**, the anti descriptor is used. In all of the anti transition structures there exists strong intramolecular (H_a−O_4) hydrogen bonding in the peracid moiety itself, in addition to the allylic hydroxy group that coordinates to the electrophilic peroxy oxygen atom O_2 that is transferred to the nucleophilic π bond. The chirality center at the allylic position in the transition structures is specified as *2R* (structures **3a**−**d**) or 2*S* (structures **3e**−**h**). Finally, for the transition structures **3a**, **3b**, **3g**, and **3h** the conformer **1b** (30° < C_4−C_3−C_2−O_1 < 55°) of the chiral allylic alcohol **1** was used, while for the transition structures **3c**, **3d**, **3e**, **3f** conformer **1a** (126° < C_4−C_3−C_2−O_1 < 136°) is involved.

The structural differences in the transition states for the epoxidation of the achiral allyl alcohol and the chiral substrate **1** derive from the allylic strain in the latter, which conformationally aligns the substrate molecule for hydrogen bonding with the oxidant. This constitutes a principal requisite for the hydroxy group directivity, as manifested through the experimentally observed threo π-facial selectivity in the epoxidation (Scheme 1). Irrespective of whether the peracid attacks the double bond from the syn or anti spiro-like orientation, it is clearly evident that $A^{1,3}$ strain between the C_1 and C_5 methyl groups (in the transition structures **3c** and **3d**) is the cause for the relatively high activation energy. Also TS-**3g** and particularly **3h** are unlikely in view of unfavorable $A^{1,2}$ strain between the C_1 and C_6 methyl groups.

Of the eight transition structures **3a**−**h** (Table 1), the lowest-energy transition state corresponds to *syn*-(2*R*,3*R*,4*S*)-TS-**3a** (erythro) with the relatively small B3LYP/6-31G(d,p) basis set. However, when the basis set includes polarization functions on the heavy atoms (6-

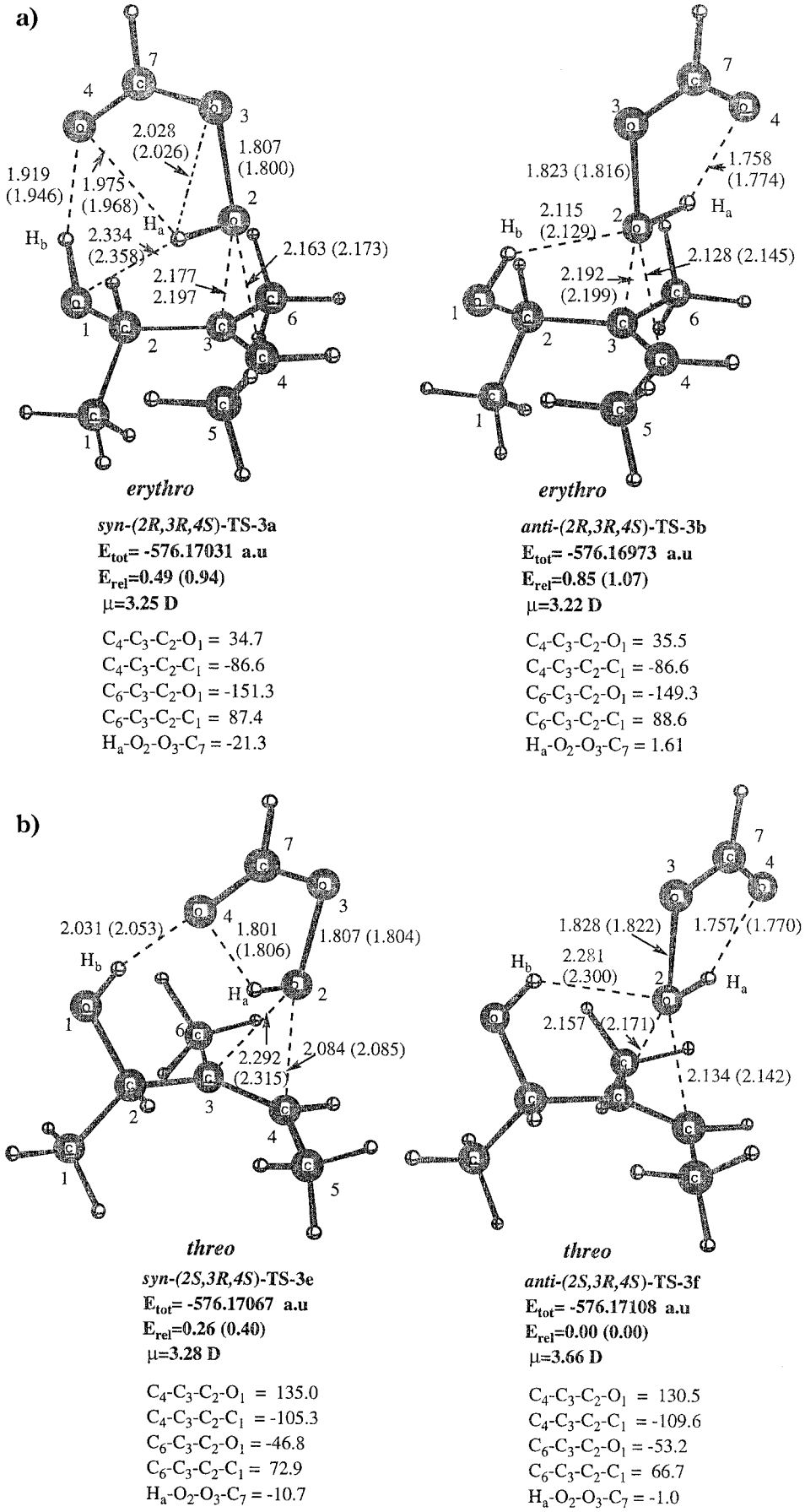

Figure 4. Lowest-energy transition structures *syn*-(2*R*,3*R*,4*S*)-TS-**3a**, *anti*-(2*R*,3*R*,4*S*)-TS-**3b**, *syn*-(2*S*,3*R*,4*S*)-TS-**3e**, and *anti*-(2*S*,3*R*,4*S*)-TS-**3f** for the epoxidation of **1**, optimized at the B3LYP/cc-pVTZ and B3LYP/AUG-cc-pVTZ (numbers in parentheses) level of theory. The relative energies (E_{rel}) are based upon total energies.

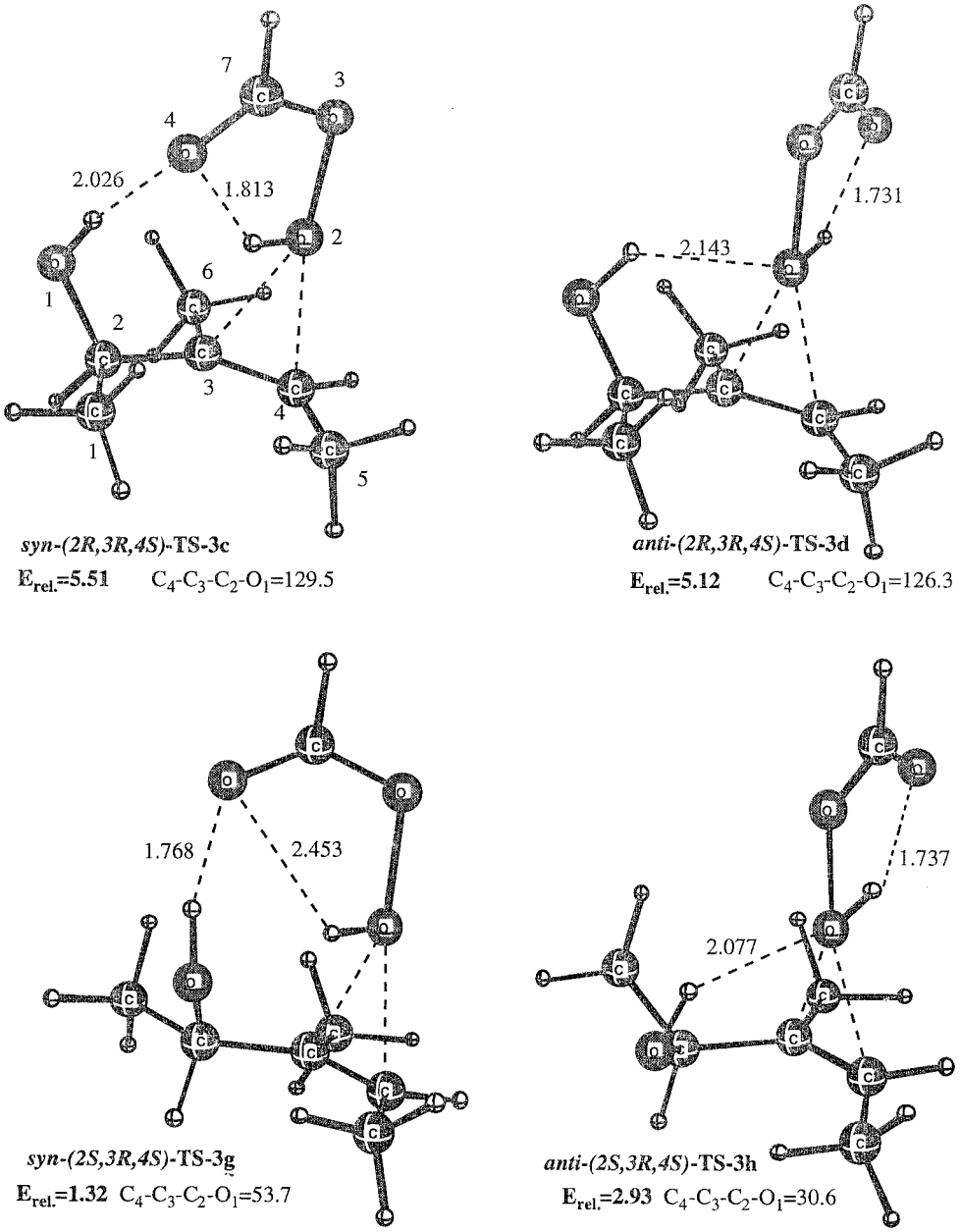

Figure 5. Higher energy transition structures *syn*-(2*R*,3*R*,4*S*)-TS-**3c,** *anti*-(2*R*,3*R*,4*S*)-TS-**3d** for the epoxidation of **1a** and transition structures *syn*-(2*S*,3*R*,4*S*)-TS-**3g**, *anti*-(2*S*,3*R*,4*S*)-TS-**3h**, for the epoxidation of **1b** optimized at the B3LYP/6-31G(d,p) level of theory. The relative energies (E_{rel}, kcal/mol) are based upon total energies and given with respect to *syn*-(2*R*,3*R*,4*S*)-TS-**3a** (which is lowest energy TS at this level).

311+G(d,p)),[15d,20] which presumably gives a better description of the oxygen lone-pair electrons, the relative order is reversed; an energy preference of ca. 1.0 kcal/mol is computed for the threo approach, namely transition structure *anti*-(2*S*,3*R*,4*S*)-TS-**3f**.

Since this is a very complex reaction coordinate with very close relative energies of the TSs, we have selected the four lowest energy TSs at the B3LYP/6-31G(d,p) level (**3a**, **3b**, **3e**, **3f**, Table 1) for re-optimization with the cc-pVTZ and AUG-cc-pVTZ basis sets (Figure 4). The relative order of reactivity between **3a** and **3f** is confirmed by the much larger augmented AUG-cc-pVTZ basis set. A basis set of this flexibility should provide an adequate description of the complex H-bonding interactions and the structural features of the TSs. All of the alternative transition structures, **3c**, **3d**, **3g**, and **3h** (Figure 5) have higher activation barriers and should contribute only marginally in controlling the threo/erythro product ratio (Table 1).

The two lowest energy (Table 2) TSs both have a threo approach of the peracid to substrate **1** that corresponds to the experimentally observed threo π-facial diastereoselectivity about the C_2-C_3 bond (Scheme 1),[4] which corroborates the hydroxy group directivity.

(19) For a description of the G2 level, see: Curtiss, L. A.; Raghavachari, K.; Trucks, G. W.; Pople, J. A. *J. Chem. Phys.* **1991**, *94*, 7221−7230.

(20) It has been suggested that satisfactory results on H-bonding interactions and in describing both structure and vibrational spectra at a correlated level may be obtained at the B3LYP/6-31+G(d,p) level of theory: Del Bene, J. E. *Hydrogen Bonding 1, Encyclopedia of Computational Chemistry*; John Wiley and Sons: New York, 1998; Vol. 2, p 1263.

Table 2. Total Energies (au) and Relative Energies (kcal/mol, Given in Parentheses) of the Transition Structures for the Epoxidation of (*Z*)-3-Methyl-3-penten-2-ol with Peroxyformic Acid at Various Levels of Theory

transition structure	B3LYP/ 6-31G*	B3LYP/ 6-31G**	QCISD(T)/6-31G* //B3LYP/6-31G**	B3LYP/6-311+G** //B3LYP/6-31G**	B3LYP/ 6-311+G**	B3LYP/cc-pVTZ //B3LYP/6-31G**	B3LYP/ cc-pVTZ	B3LYP/ AUG-cc-pVTZ
erythro-**3a**	−575.93626	−575.96371	−574.29349	−576.12535	−576.12599	−576.16964	−576.17030	−576.17870
syn-(2*R*,3*R*,4*S*)[a]	**(0.00)**	**(0.00)**	**(0.00)**	(1.05)	(1.01)	(0.56)	(0.49)	(0.94)
erythro-**3b**	−575.93403	−575.96177		−576.12541	−576.12595	−576.16919	−576.16973	−576.17850
anti-(2*R*,3*R*,4*S*)[b]	(1.40)	(1.22)		(1.01)	(1.04)	(0.84)	(0.85)	(1.07)
threo-**3e**	−575.93469	−575.96220		−576.12549	−576.12604	−576.17010	−576.17067	−576.17956
syn-(2*S*,3*R*,4*S*)	(0.99)	(0.95)		(0.96)	(0.98)	(0.26)	(0.26)	(0.40)
threo-**3f**	−575.93485	−575.96254	−574.29292	−576.12702	−576.12760	−576.17053	−576.17108	−576.18020
anti-(2*S*,3*R*,4*S*)	(0.88)	(0.74)	(0.36)	**(0.00)**	**(0.00)**	**(0.00)**	**(0.00)**	**(0.00)**

[a] The syn orientation has the alcohol OH hydrogen bonded to the carbonyl oxygen atom. [b] The anti orientation has the alcohol OH hydrogen bonded to the distal peroxy oxygen atom.

In the lowest energy TS, *anti*-(2*S*,3*R*,4*S*)-TS-**3f** (Figure 4b), the **1a** conformer of the allylic alcohol **1** has the *Si* face of the C_3-C_4 π-bond attacked that is supported by the H_b-O_2 (2.300 Å) hydrogen bond (all the numbers given here correspond to the highest level B3LYP/AUG-cc-pVTZ optimized structures). The peroxyformic acid is essentially planar ($H_a-O_2-O_3-C_7 = -1.7°$) and approaches the double bond in a nearly perfect spiro orientation ($C_3-C_4\sim O_3-O_4 = -94.9°$) with an anti orientation of the peracid moiety with respect to the hydroxyl functionality of the allylic alcohol (i.e., the hydrogen-bonding interaction involves the distal peroxy oxygen atom O_2). The *threo*-TS-**3e** is only 0.40 kcal/mol higher in energy, but it has a syn orientation of the peracid with a H-bonding interaction to the carbonyl oxygen atom O_4. Thus, there is very little distinction energetically between the H-bonding interactions of the directing hydroxyl group with the carbonyl oxygen O_4 or the distal peroxy oxygen[10] atom O_2 for the syn and anti orientations of the peracid in the threo TSs. We find this to be a surprising result since G2 theory[19] suggests that the proton affinity of the carbonyl oxygen atom O_4 in peroxyformic acid (PA_{298} = 177.1 kcal/mol) is 23.1 kcal/mol greater at 0 K (23.8 at 298 K) than its adjacent peroxy oxygen atom O_3.[9a] While this enhanced carbonyl oxygen basicity is reflected in the greater stability of ground-state complexes **2b** and **2d**, it does not translate to the transition structures where the peroxy oxygen is slightly favored.

The *erythro*-TS-**3a** (Figure 4, Part 1) also has the syn orientation, and its relative energy is 0.94 kcal/mol with respect to TS-**3f**. The 2*R*-configured **1b** conformer of allylic alcohol **1** in *syn*-(2*R*,3*R*,4*S*)-TS-**3a** is attacked preferentially from the *Si* face of the C_3-C_4 π-bond, assisted by two effective H_a-O_1 (2.352 Å) and H_b-O_4 (1.946 Å) hydrogen-bonding interactions. The latter is facilitated through the syn orientation of the peroxy carbonyl oxygen atom (O_4) in the spiro-like attack and the propitious $C_4-C_3-C_2-O_1$ dihedral angle of 35.3°, which leads finally to the 2*R*,3*R*,4*S* epoxide. The other *erythro*-TS-**3b** is 1.07 kcal/mol higher in energy than TS-**3f,** but it has the anti orientation of the peracid.Thus, the directing effect of the alcohol group may involve H-bonding interactions with either the peroxy or the carbonyl oxygens with essentially equal probability irrespective of the conformation of allylic alcohol **1** that participates. The good agreement with experiment is gratifying, especially when such small energy differences are involved, since the experimental threo/erythro ratio of 90:10 (Scheme 1) corresponds to a $\Delta\Delta G^{\ddagger} = 1.3$ kcal/mol.

The *anti*-(2*S*,3*R*,4*S*)-TS-**3f** transition state is a precursor for the traditional 1,4-hydrogen shift established in peracid epoxidations.[9a] Dynamic visualization of the vectors of the single imaginary frequency [371i cm^{-1}, B3LYP/6-31G(d)] shows principally O_2-O_3 bond elongation as the electrophilic O_2 oxygen atom oscillates between the proximal O_3 peroxy oxygen atom and the approximate center of the C_3-C_4 double bond. There is essentially no motion of the acidic peroxy hydrogen atom H_a, its bond distance merely lengthens slightly as the electrophilic OH group approaches the nucleophilic π bond. Little motion of the C_5 and C_6 methyl groups or the developing carboxylate functionality $O_3-C_7-O_4$ is displayed. Animation of *syn*-(2*R*,3*R*,4*S*)-TS-**3a** [384i cm^{-1}, B3LYP/6-31G(d)] indicates similar behavior with additional rocking motion of the hydrogen atom H_b in the allylic alcohol **1**, but it does not appear to approach the carbonyl oxygen atom O_4 any closer.

Transition structures *syn*-(2*R*,3*R*,4*S*)-TS-**3a** and *syn*-(2*S*,3*R*,4*S*)-TS-**3e** closely resemble $\mathbf{TS_{AA}}$ for the epoxidation of allyl alcohol[9a] (Figure 1), but presumably steric interactions in the more complex transition structures for the epoxidation of methyl-substituted allylic alcohol **1** do not affect the H-bonding interactions to either of the peracid oxygen atoms involved. Comparison of the O_2-O_3 distances suggests that TS-**3f** and TS-**3b** are later along the reaction coordinate with a stronger H_a-O_4 hydrogen bond. This may be a reason for the lowering of their relative energy with respect to transition structures **3e** and **3a**.

Another significant observation that pertains to the geometrical features of transition state *syn*-(2*R*,3*R*,4*S*)-TS-**3a** optimized with the 6-31G(d,p) versus the AUG-cc-pVTZ basis set is that the larger basis set produces a more planar peroxyformic acid moiety. The $H_a-O_2-O_3-C_7$ dihedral angle reduces from −49.1°(6-31G(d,p)) to −20.4° (AUG-cc-pVTZ) (Table 3), whereas in the case of $\mathbf{TS_{AA}}$ it is −14.9°.

Hydrogen atom H_a is appreciably more displaced from the peracid plane in the direction of the allylic hydroxy group for the *syn*-(2*R*,3*R*,4*S*)-TS-**3a** at 6-31G(d,p) than for *syn*-(2*R*,3*R*,4*S*)-TS-**3a** at cc-pVTZ and AUG-cc-pVTZ (Figures 5 and 6) and $\mathbf{TS_{AA}}$ (Figure 1). On the contrary, when the peracid moiety is essentially planar as in TS-**3f,** the $H_a-O_2-O_3-C_7$ dihedral angle, which ranges from −1.7 to 0.7°, is unaffected by the various basis sets. The distances between H_a-O_3 and H_a-O_4 are also highly dependent upon the basis set used. With the 6-31G(d,p) basis set we obtained H_a-O_3 = 2.074 Å and H_a-O_4 = 2.398 Å (similar distances have been calculated at 6-311+G(d,p), Table 3) which predict a 1,2 hydrogen shift (H_a prefers to migrate to O_3) recently proposed as an operative pathway for similar structures.[10b]

This pathway has been supported in this study as well by intrinsic reaction coordinate following (IRC)[11c,d] cal-

Table 3. Comparison of the Selected Interatomic Distances (Å) and Dihedral Angles (Deg) in the Lowest Energy *threo-anti*-(2*S*,3*R*,4*S*)-3f and *erythro-syn*-(2*R*,3*R*,4*S*)-3a Transition Structures Optimized at Different Levels of Theory

geometry	B3LYP/ 6-31G*	B3LYP/ 6-31G**	B3LYP/ 6-311+G**	B3LYP/ cc-pVTZ	B3LYP/ AUG-cc-pVTZ	MP2/ 6-31+G**
			anti-(2*S*,3*R*,4*S*)-**3f**			
C4−O2	2.15	2.15	2.17	2.13	2.14	2.17
C3−O2	2.14	2.15	2.19	2.15	2.17	2.09
O2−O3	1.82	1.82	1.82	1.83	1.82	1.76
C3−C4	1.38	1.38	1.38	1.37	1.37	1.38
H_a−O4	1.76	1.76	1.81	1.76	1.78	1.85
H_b−O2	2.17	2.18	2.25	2.28	2.30	2.16
H_b−O3	2.81	2.84	2.92	2.96	2.99	2.69
C4−C3−C2−O1	128.8	129.5	129.7	130.5	130.5	132.7
H_a-O2-O3−C7	−0.4	−0.3	−1.5	−1.0	−1.7	0.7
C3−C4∼O3−O4[a]	−92.2	−92.9	−95.5	−93.8	−94.9	−94.8
			syn-(2*R*,3*R*,4*S*)-**3a**			
C4−O2	2.13	2.16	2.22	2.16	2.17	
C3−O2	2.10	2.10	2.16	2.18	2.20	
O2−O3	1.82	1.82	1.81	1.81	1.80	
C3−C4	1.38	1.38	1.37	1.37	1.37	
H_a−O4	2.47	2.40	2.33	1.98	1.97	
H_a−O3	2.08	2.07	2.08	2.03	2.03	
H_a−O1	1.90	1.98	2.18	2.33	2.35	
H_b−O4	1.78	1.75	1.86	1.92	1.95	
C4−C3−C2−O1	54.6	43.2	41.4	34.7	35.4	
H_a-O2-O3−C7	−55.5	−49.1	−44.8	−21.3	−20.4	
C3−C4∼O3−O4[a]	35.8	44.2	52.2	66.3	66.5	

[a] Dihedral angle between nonbonded atoms indicates the spacial arrangement of the peroxyformic acid "plane" (based upon O3, C7, and O4 atoms) with respect to the plane of the substrate alcohol (based upon C2, C3, and C4 atoms).

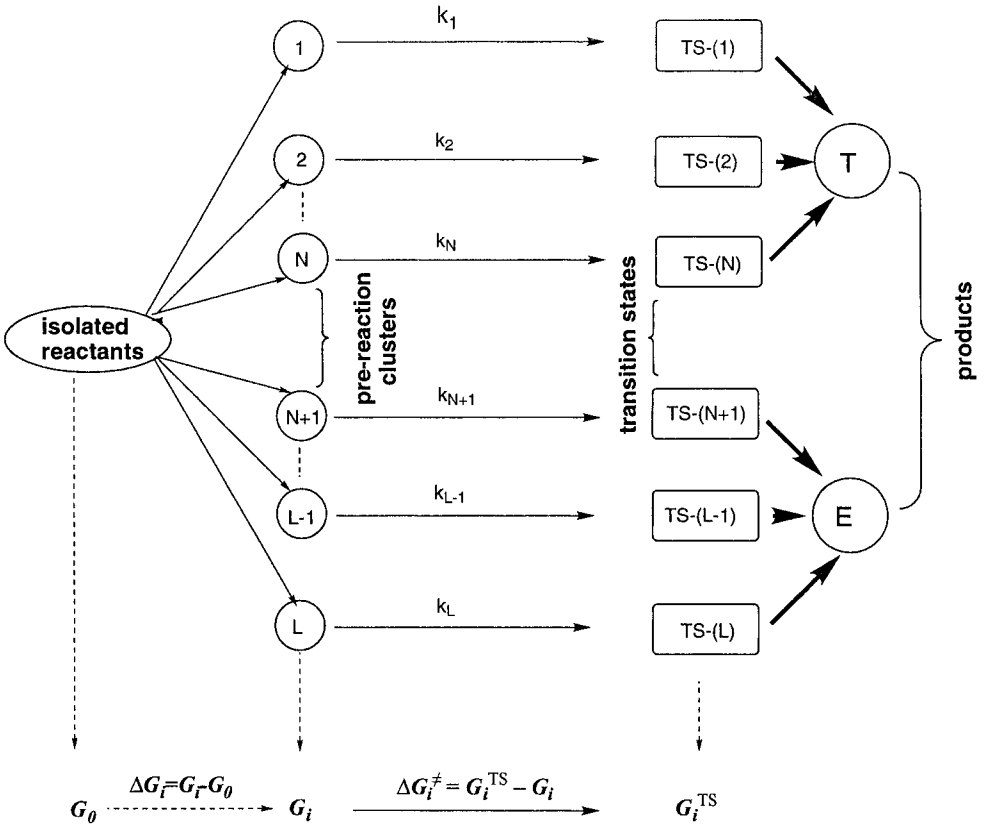

Figure 6. Multi-transition-state reaction for the formation of the two products **T** and **E** (threo and erythro, for instance). The pre-reaction clusters 1,2,...N lead to the **T** product through the corresponding transition states TS-(1), TS-(2),...TS-(*N*) with the rate constants k_1, k_2,...k_N. The pre-reaction clusters $N + 1$,...$L - 1$, L lead to the **E** product through the corresponding transition states TS-($N + 1$)...TS-($L - 1$), TS-(L) with the rate constants k_{n+1},... k_{L-1},k_L.

culations at B3LYP/6-31G(d) level of theory (illustrated in Figure S2, Supporting Information).

In the case of $\mathbf{TS_{AA}}$ (Figure 1), the distance H_a-O_3 is longer than H_a-O_4, and the traditional 1,4 hydrogen shift was found.[9a] Since *syn*-(2*R*,3*R*,4*S*)-TS-**3a**, optimized with the AUG-cc-pVTZ basis set (Figure 4a), has H_a-O_3 = 2.026 Å and H_a-O_4 = 1.968 Å (Table 3), it is highly likely that this structure will exhibit the same mechanistic behavior (1,4-H shift) as $\mathbf{TS_{AA}}$. Then the novel pathway involving a 1,2-hydrogen shift[10b] would be simply an

artifact of using a small basis set that distorts the geometry of the peracid moiety errantly and results in hydrogen migration to the nearest oxygen atom. Thus, one should be very careful about mechanistic conclusions based on the results of a few optimizations when such nonplanar structures with a complex H-bonding network are involved. Re-optimizations of this type of H-bonded structure at the highest possible levels of theory are highly recommended. It is well-known that the use of the small basis sets often overestimates the extent of hydrogen bonding and may, thus, significantly distort nonplanar geometries of the peracid if hydrogen-bonding interactions are favored energetically. This is also presumably the reason for the greater stability of TS-**3a** at 6-31G** (lowest energy) which is reversed with the more diffuse 6-311+G(d,p) and AUG-cc-pVTZ basis sets.

The use of the higher-level B3LYP single-point computations on the B3LYP/6-31G(d,p) optimized structures (Table 2, compare four last columns) does not change markedly the relative energies of the transition states in comparison with the full optimization results at the same levels. However, as we have shown above for TS-**3a,** its geometry is basis set dependent (Table 3), and transition structure optimization with the smaller basis set can lead to serious mechanistic misunderstandings. Contrawise, the transition state geometries are not significantly affected by the basis set choice when the peroxyformic acid moiety is planar. Table 3 compares bond distances in the key **3a** and **3f** transition structures with the various basis sets. It is seen that in contrast to the MP2 method, all the B3LYP optimizations of **3f** produce a similar geometry with the symmetrical approach of the peroxy oxygen atom (the asymmetric approach of the peroxyformic acid is an artifact of the MP2 method [9]).

Evaluation of the Threo/Erythro Product Ratio Based upon the Extended Curtin−Hammett Principle. Now we shall consider the thermodynamic properties of ground-state pre-reaction clusters and their corresponding transition structures **3a**−**f**. In view of such small computed energy gaps between the transition states, for the estimation of the threo/erythro product ratio, all four lowest-energy transition structures, **3a**, **3b**, **3e**, and **3f**, will contribute to the product ratio.

The competition between the lowest energy threo and erythro transition structures constitutes a classic example of the Curtin−Hammett (C−H) principle.[21a] The position of the conformational equlibrium cannot control the product ratio, since the major product may arise through the reaction of the minor pre-reaction cluster if it has the lowest activation barrier. As noted earlier by Narula,[22] based upon an analysis of the diastereomeric transition states for stereoselective epoxidation of acyclic allylic alcohols, the product ratio is controlled by the Curtin−Hammett principle, provided that the complexation-decomplexation between the olefin and the peracid is reversible and faster than the rate of epoxidation (the barriers are listed in Table 1).

Usually the Curtin-Hammett principle is given for two competitive transition states. For the present multi-transition-state system, we will extend it according to the generalized scheme shown in Figure 6. Let us consider the reaction system with $i = \overline{1,L}$ transition states which can lead to either the T*(threo)* ($i = \overline{1,N}$) or E *(erythro)* product ($i = \overline{N+1,L}$). The transition states and reactants have their total free energies denoted by G_i^{TS} and G_i.

According to transition state theory, the rate constant for each individual reaction i is given by eq 1

$$k_i = C \times \exp(-\Delta G_i^{\neq}/RT) \tag{1}$$

in which $C = æk_BT/h$ (æ is the transmission coefficient, k_B is Boltzmann's constant, h is Planck's constant, T is the absolute temperature) and $\Delta G_i^{\ddagger} = G_i^{TS} - G_i$.

The ground-state population of each pre-reaction cluster (p_i) is determined by the Boltzmann distribution and may be expressed in terms of the free energy differences ($\Delta G_i = G_i - G_0$) with respect to some fixed free energy, G_0 (which may be the free energy of the isolated reactants). Thus, p_i is given by eq 2

$$p_i = p_0 \times \exp(-\Delta G_i/RT) \tag{2}$$

Since $\sum_{i=1}^{L} p_i = 1$, it follows from eq 2 that

$$p_i = \exp(-\Delta G_i/RT)/\sum_{i=1}^{L}\exp(-\Delta G_i/RT) \tag{3}$$

The product ratio for this multipath reaction may be determined by eq 4, which follows from eqs 1 and 3 and holds if the Boltzmann distribution of the pre-reaction clusters is not disturbed during the reaction course.

$$\frac{[T]}{[E]} = \frac{p_1k_1 + p_2k_2 + ... + p_Nk_N}{p_{N+1}k_{N+1} + p_2k_2 + ... + p_{L-1}k_{L-1} + p_Lk_L} = \frac{\sum_{i=1}^{N}\exp(-(\Delta G_i + \Delta G_i^{\neq})/RT)}{\sum_{j=N+1}^{L}\exp(-(\Delta G_j + \Delta G_j^{\neq})/RT)} \tag{4}$$

If only two conformers are involved, the product ratio is given by the fundamental precursor to the classical C−H principle expression eq 4a:

$$[T]/[E] = K_{eq}k_1/k_2 \tag{4a}$$

It should be noted that eq 4a explicitly states that the [T]/[E] product ratio equals the product of the equilibrium constant K_{eq} times the ratio of the two rate constants k_1 and k_2. This form of the C−H principle, where the conformational preference plays a direct role, is often overlooked because this same product ratio may be simply derived from the free energies of the transition structures as derived below.[23]

Substitution of $\Delta G_i = G_i - G_0$ and $\Delta G_i^{\neq} = G_i^{TS} - G_i$ into eq 4 leads to the product ratio based upon the free

(21) (a) Curtin, D. Y. *Rec. Chem. Prog.* **1954**, *15*, 111−128. (b) Seeman, J. I. *Chem Rev.* **1983**, *83*, 84−134.

(22) Narula, A. S. *Tetrahedron Lett.* **1981**, *22*, 2017−2020.

(23) (a) For an excellent discussion of the controversy surrounding the Curtin−Hammett principle and its amendment of the original version by the IUPAC see ref 21b. (b) Equation 6a inherently takes the population of reactants into account. A free energy equal to $\Delta G°$, the free energy difference between the two rapidly equilibrating conformers (reactants) must be added to the activation barrier for the higher energy TS: $\Delta G^{TS} = \Delta G_1^{\ddagger} + \Delta G° - \Delta G_2^{\ddagger}$ and $[T]/[E] = \exp(-(\Delta G_1^{\ddagger} + \Delta G° - \Delta G_2^{\ddagger})/RT) = \exp(-\Delta G^{TS}/RT)$.

Table 4. Classical Energies (E_{rel}^{TS}), Enthalpies (H_{rel}^{TS}), and Free Energies (G_{rel}^{TS}) at 298.15 K (kcal/mol) of the Transition Structures (Relative to the Lowest Energy TS-3f) for the Epoxidation of (*Z*)-3-Methyl-3-penten-2-ol with Peroxyformic Acid. (The B3LYP Method with Various Basis Sets Was Used and the Product Distribution Ratio Threo/Erythro Was Derived from Eq 6. The Thermochemical Data for the Computation of H_{rel}^{TS} and G_{rel}^{TS} Were Taken from B3LYP/6-31G(d) Frequency Calculations)

transition structure	E_{rel}^{TS} 6-311+G**	H_{rel}^{TS} 6-311+G**	G_{rel}^{TS} 6-311+G**	E_{rel}^{TS} AUG-cc-pVTZ	H_{rel}^{TS} AUG-cc-pVTZ	G_{rel}^{TS} AUG-cc-pVTZ
erythro-**3a** *syn*-(2*R*,3*R*,4*S*)[a]	1.01	1.21	2.27	0.94 (0.49)[d]	1.14 (0.69)	2.21 (1.76)
erythro-**3b** *anti*-(2*R*,3*R*,4*S*)[b]	1.04	1.00	1.05	1.07 (0.85)	1.04 (0.82)	1.08 (0.86)
threo-**3e** *syn*-(2*S*,3*R*,4*S*)	0.98	1.13	1.67	0.40 (0.26)	0.55 (0.41)	1.10 (0.95)
threo-**3f** *anti*-(2*S*,3*R*,4*S*)	0.00	0.00	0.00	0.00	0.00	0.00
threo/erythro[c]	3.4	3.7	5.5	4.1 (2.4)	4.4 (2.7)	6.2 (4.2)

[a] The syn orientation has the alcohol OH hydrogen bonded to the carbonyl oxygen atom. [b] The anti orientation has the alcohol OH hydrogen bonded to the distal peroxy oxygen atom. [c] Product ratio calculated by eq 6. [d] Numbers in parentheses correspond to the B3LYP/cc-pVTZ full optimization.

energies:

$$\frac{[T]}{[E]} = \frac{\sum_{i=1}^{i=N} \exp(-(G_i^{TS} - G_o)/RT)}{\sum_{j=N+1}^{L} \exp(-(G_i^{TS} - G_o)/RT)} = \frac{\sum_{i=1}^{N} \exp(-G_i^{TS}/RT)}{\sum_{j=N+1}^{L} \exp(-G_j^{TS}/RT)} \quad (5)$$

Let us assume that the first ($i = 1$) TS is the lowest energy one among all L transition states. Dividing both sides of the [T]/[E] ratio in eq 5 by $\exp(-G_1^{TS}/RT)$, we obtain the expression in eq 6, (which will be used for the calculation of the threo/erythro ratio based upon the data presented in Table 4)

$$\frac{[T]}{[E]} = \frac{1 + \sum_{i=2}^{N} \exp(-G_{rel.i}^{TS}/RT)}{\sum_{j=N+1}^{L} \exp(-G_{rel.j}^{TS}/RT)} \quad (6)$$

in which $G_{rel.i}^{TS} = G_i^{TS} - G_1^{TS}$ is the relative free energy of the *i*th transition structure [TS-(i)] with respect to the lowest-energy transition structure (e.g., TS-**3f**).

This expression reduces to the simplified version of the Curtin−Hammett principle if one has only two transition states with the total free energies G_1 and G_2, which lead to the *T* and *E* products. Then eq 5 transforms into eq 6a, which is the typical expression for the Curtin−Hammett equation *and the mathematical equivalent of eq 4a*.[21b]

$$\frac{[T]}{[E]} = \frac{\exp(-G_1^{TS}/RT)}{\exp(-G_2^{TS}/RT)} = \exp[-(G_1^{TS} - G_2^{TS})/RT] = \exp(\Delta G^{TS}/RT) \quad (6a)$$

The eq 4a[21b] relates the product composition to experimentally (or in this case theoretically) measurable quantities such as equilibrium constants and rate constants, while eq 6a predicts the product distribution based upon the *difference* in the free energy between two transition states ΔG^{TS}. The latter quantity is not an experimentally observable quantity but rather is derived from rate constants and equilibrium constants. In a pragmatic sense, eq 4a[21b] provides a better understanding of the overall reaction, as demonstrated below.

To get the product ratio for our case, it is necessary to calculate the relative free energies for the localized transition structures **3a**−**f** (Table 1 and Table S1 in the Supporting Information). Table 4 reports the relative data for **3a**−**f** based upon the total energies (E_{rel}), enthalpies (H_{rel}), and free energies (G_{rel}) calculated at 298.15 K with 6-311+G (d, p), cc-pVTZ, and AUG-cc-pVTZ basis sets and the thermodynamic quantities (entropy and thermal correction) from B3LYP/6-31G(d) frequency calculations. The use of thermal corrections and entropies leads to "destabilization" of transition structures **3a** and **3e** (1.3 kcal/mol 0.7 kcal/mol). This results in an increase in the threo/erythro ratio when using free energy data and eq 6: at B3LYP/cc-pVTZ the ratio is changed from 2.4 (based upon E_{rel} data) to 4.2 (for G_{rel} results). Because the calculated relative energies are now even smaller, we were prompted to use an augmented AUG-cc-pVTZ basis set as a more stringent examination of the role that intramolecular H-bonding plays in the rate-limiting oxygen transfer step. The calculated threo/erythro ratios at this level of 4.1 (when using E_{rel} data) and 6.2 (for G_{rel} results) provide the best agreement with the experimental ratio 90:10.

For a better understanding of the overall energetic picture we illustrate the relative energetic positions of the transition states and the corresponding pre-reaction clusters in Figure 7.

As seen from the data presented in Figure 7, the major threo product is derived from *anti*-TS-**3f** (67%) and *syn*-TS-**3e** (13%) which is in good agreement with the experimental threo/erythro product ratio of 90:10. Pre-reaction cluster **2b** is present in the highest concentration, i.e., 62%, but since it has the highest activation barrier for epoxidation (16.9 kcal/mol), it makes the smallest contribution (4%) to the overall product composition. Likewise, pre-reaction cluster **2c** is only present in 1%, but its relatively low activation barrier (13.45 kcal/mol) affords the major portion of the erythro product (16%). With an SCIPCM solvent correction of the free energies the threo/erythro product ratio of 86:14 is quite comparable. We also included the [T]/[E] product ratio

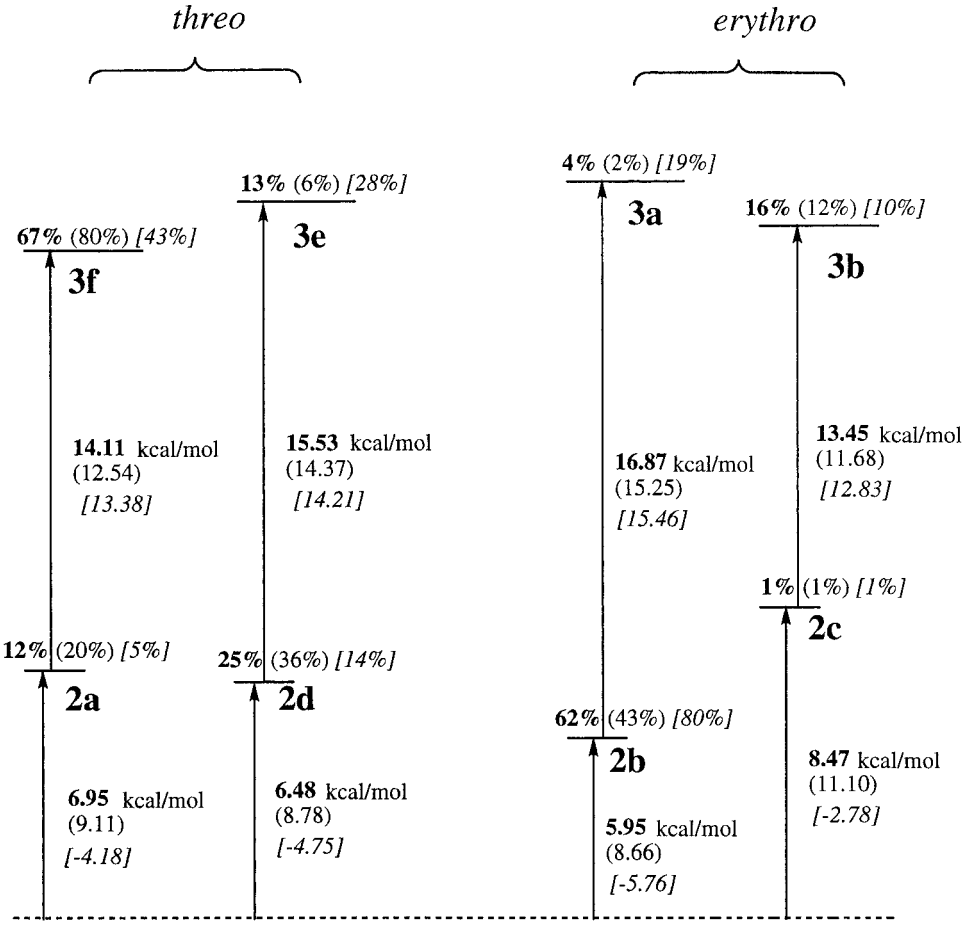

Figure 7. Free energies (kcal/mol) and product composition (%) based upon the B3LYP/cc-pVTZ calculations presented in Table 1; the values in bold are derived from the data in the 8th column, the values in parentheses are solvent corrected (SCIPCM model) and are derived from the data in the 10th column, and values in brackets are without entropy and thermal corrections and are derived from the data in the fourth column of Table 1.

Table 5. Calculated Solvent (ϵ = 8.9 for CH_2Cl_2) Stabilization Energies (kcal/mol) with Different Solvent Models by Using the Equation $\delta E_{solv} = E_{tot}$(solvent) − E_{tot}(Gas Phase)

transition structure[a]	mode of H-bonding	μ^b B3LYP/ cc-pVTZ	μ^b B3LYP/ 6-311+G**	μ^b B3LYP/ 6-31G**	PCM, B3LYP/ 6-31G*	PCM, B3LYP/ 6-311+G**	SCIPCM, B3LYP/ 6-31G*
erythro-**3a** *syn*-(2*R*,3*R*,4*S*)	$H_b\cdots O_4{=}C_7$	3.25 (3.44)[c]	3.68	3.73	−4.61	−5.31	−5.01
erythro-**3b** *anti*-(2*R*,3*R*,4*S*)	$H_b\cdots O_2{-}C_3$	3.22 (3.42)	3.34	3.07	−4.41	−4.90	−5.25
threo-**3e** *syn*-(2*S*,3*R*,4*S*)	$H_b\cdots O_4{=}C_7$	3.28 (3.49)	3.34	3.12	−3.73	−4.09	−4.97
threo-**3f** *anti*-(2*S*,3*R*,4*S*)	$H_b\cdots O_2{-}C_3$	3.66 (3.77)	3.87	3.48	−4.38	−4.96	−5.52

[a] The transition structures for single-point solvent effect calculations were optimized at the B3LYP/6-31G** level. [b] The values of the dipole moments, μ (in Debye), have been calculated through Mulliken population analysis performed at the final stage of the optimization. [c] The values of dipole moments given in parentheses are calculated with the AUG-cc-pVTZ basis set using B3LYP/cc-pVTZ-optimized structures.

based upon calculated total energies (classical barriers, $\Delta E^{\ddagger}$), for which the threo/erythro product ratio is of 71:29. It is gratifying to see that all three methods are in such good agreement with each other and with experiment.

Solvent Simulations. Since the experimental data for this reaction involve solvation effects, we have examined the reaction in solution with the Tomasi's PCM[17a] model and the self-consistent isodensity model (SCIPCM)[17b] using the dielectric constant for CH_2Cl_2 (Tables 5 and 6).

From the values of the calculated dipole moments presented in Table 5, it is readily seen that the relative charge distributions in structures TS-**3a**−**f** depends on the basis set used. In particular, TS-**3a** has the largest dipole moment at 6-31G(d, p), but at cc-pVTZ and AUG-cc-pVTZ its dipole moment is close to that of **3b** and **3e**, whereas TS-**3f** always has a dipole moment approximately 0.4 D higher than transition structures **3b** and **3e**. Since the larger basis set produces the highest dipole moment for **3f**, one might logically expect that the transition structure **3f** should be more highly stabilized by polar solvents than the other transition structures. The SCIPCM method supports this expectation, as evidenced by the data listed in Table 5. The PCM model, always favors structure **3a**, which has the highest dipole moment (for the 6-31G(d,p) basis set). It is also interesting to notice that PCM calculations of stabilization energies with the 6-311+G (d, p) basis set result in the same (0.6 kcal/mol) increase in the stabilization of TS-

Table 6. Calculated Relative Free Energies (G_{rel}^{TS}, kcal/mol) of the Transition Structures 3a,b,e,f (with Respect to the Lowest Energy TS-3f) and the Threo/Erythro Product Ratio with the Correction for the Solvent Stabilizing Effect (CH_2Cl_2) Computed within Different Solvent Models (see Table S1)

transition structure	B3LYP/ 6-311+G** PCM, B3LYP/ 6-31G**	B3LYP/ 6-311+G** PCM, B3LYP/ 6-311+G**	B3LYP/ 6-311+G** SCIPCM, B3LYP/ 6-31G*	B3LYP/ AUG-cc-pVTZ, PCM, B3LYP/ 6-31G**	B3LYP/ AUG-cc-pVTZ, PCM, B3LYP/ 6-311+G**	B3LY/ AUG-cc-pVTZ, SCIPCM, B3LYP/ 6-31G*
erythro-**3a** *syn*-(2*R*,3*R*,4*S*)	2.04	1.92	2.79	1.98 (1.52)[a]	1.86 (1.40)	2.72 (2.26)
erythro-**3b** *anti*-(2*R*,3*R*,4*S*)	1.02	1.10	1.32	1.06 (0.83)	1.14 (0.91)	1.36 (1.14)
threo-**3e** *syn*-(2*S*,3*R*,4*S*)	2.33	2.54	2.22	1.75 (1.61)	1.97 (1.82)	1.65 (1.50)
threo-**3f** *anti*-(2*S*,3*R*,4*S*)	0.00	0.00	0.00	0.00	0.00	0.00
threo/erythro	**4.9**	**5.2**	**8.8**	**5.2 (3.3)**	**5.5 (3.4)**	**9.5 (6.4)**

[a] The numbers in parentheses are based upon the total energies of the B3LYP/cc-pVTZ fully optimized TSs.

3a and TS-**3f** (in comparison with the 6-31G(d,p) stabilization energies).

Another assumption on the solvent effect follows from a comparison of the different modes of H-bonding of the allylic hydroxy group to peroxyformic acid. The proton affinity, according to G2 calculations,[9a] is much larger for the carbonyl oxygen atom O_4 than for the distal peroxy one O_2. This suggests that gas-phase H-bonding to O_4 should be stronger and as it is seen from the geometries (Figure 5 and Table 3), the $H_b\cdots O_4$ distances in **3a** and **3e** (1.946 and 2.053 Å) are always shorter than $H_b\cdots O_2$ in the transition structures **3b** and **3f** (2.129 and 2.300 Å). Naturally, solvent molecules will surround the hydroxy group and in the condensed phase this should appreciably disrupt these H-bonding interactions. Thus, the *syn* structures with the $H_b\cdots O_4$ interaction should suffer from the solvation effects more than the anti structures and, therefore, their stabilization by the solvent should be compared to the structures with $H_b\cdots O_2$ interactions. Unfortunately, these SCRF models do not explicitly treat H-bonding interactions, but nonetheless, the last column of the Table 5 (SCIPCM results) agrees well with these qualitative trends. Both PCM calculations show the smallest stabilization for the *syn*-**3e** structure but the largest stabilization for the *syn*-**3a** case.

Finally, the data in Table 6 suggest that the inclusion of solvent effects provides threo/erythro product ratios in better accord with the experimental ones (90:10, Scheme 1) than the gas-phase calculations. The use of the SCIPCM model results in an increase in the gas-phase ratio from 6.2 (Table 4) to 9.5 (Table 6) in the CH_2Cl_2 solvent, whereas the PCM model works in the opposite direction, i.e., this ratio is reduced to 5.2 and 5.5 (Table 6). The data for the cc-pVTZ and 611+G(d,p) calculations reveal the same qualitative trend. Thus, the SCIPCM model calculations correlate well with the expectations based on the experimental threo/erythro ratio and the gas-phase estimations. Inclusion of SCIPCM solvent corrections increases the threo/erythro product ratio, but the PCM model leads to the opposite conclusion.

Conclusions

We conclude from these computational data that an intricate hydrogen-bonding network between *the peroxy acid and the allylic alcohol* is responsible for directing the diastereoselectivity in the epoxidation of chiral allylic alcohols. The structural features, dictated by allylic strain and hydrogen bonding, that underline the hydroxy-group directivity for the stereochemical probe **1** could have hardly been anticipated intuitively and underscore the power of modern state-of-the-art computational methods to help elucidate more complex reaction pathways in oxygen-transfer chemistry.

Of the eight options **3a**−**h**, the four lowest-energy TSs **3a**, **3b**, **3e**, and **3f** contribute to epoxide formation. The *anti*-(2*S*,3*R*,4*S*)-TS-**3f** transition structure is the best compromise between $A^{1,2}$ and $A^{1,3}$ strains (according to the free energy data at the B3LYP/AUG-cc-pVTZ level it is 74% populated). The approach of the peracid onto the C=C bond is spiro in nature in which the dominant hydroxy-group directivity manifests itself in a hydrogen-bonding interaction between the allylic hydroxy group and the distal peroxy oxygen atom of the peracid.[10] Three additional transition states [*threo*-**3e** (12%)**,** *erythro*-**3a** (2%) and *erythro*-**3b** (12%)] contribute as well to the product distribution. The subtle balance between between $A^{1,2}$ and $A^{1,3}$ strain and different modes of H-bonding that appear to be involved in the diastereoselective epoxidation of allylic alcohols make it difficult to rationalize such small differences effect on the final product distribution. Thus, an extended Curtin−Hummett expression has been developed to estimate the threo/erythro product ratio from the present computational results. It has been shown that this approach is in line with the Self-consistent Isodensity modeling (SCIPCM) results and is in surprisingly good agreement with experiment, despite the relatively small energy differences involved.

The relative energies of the all structures and geometrical features of the nonplanar transition states with complex network of H-bonds are quite sensitive to the basis set used in the computations. Thus, it is highly recommended to use relatively large basis sets with both polarization and diffuse functions.

A 1,2 migration[10b] of the peracid hydrogen atom H_a to the peroxy oxygen atom O_3 in concert with the O−O bond cleavage suggested for nonplanar *syn*-(2*R*,3*R*,4*S*)-TS-**3a** is most likely just an artifact of the 6-31G(d,p) basis set.

The present DFT computations confirm that the chiral allylic alcohol **1** serves as a valuable stereochemical probe to elucidate mechanistic fine structure in oxygen-transfer processes. Indeed, an enlightening lesson is to be learned from the present computational exercise on the geometrical features of the pre-reaction clusters and transition structures in the peracid epoxidation of the chiral allylic alcohol **1**. Ground-state pre-reaction clusters are

not reliable criteria to assess the likely transition structure responsible for the experimentally observed *threo* diastereoselectivity. For a complete mechanistic understanding of a reaction of this complexity, detailed studies of all the intermediates and transition structures are essential with highly flexible basis sets.

Acknowledgment. The work in Newark was supported by the National Science Foundation (CHE-9901661) and in Würzburg by the Deutsche Forschungsgemeinschaft (Schwerpunktprogramm "Peroxidchemie") and the Fonds der Chemischen Industrie. We are also thankful to the National Centers for Supercomputing Applications at Urbana, IL, and Lexington, KY, for generous amounts of computer time.

Supporting Information Available: Table S1 (total energies and related thermochemical data of peroxyformic acid, the principle conformers **1a** and **1b** of the allylic alcohol substrate**,** the transition structures **3a**−**h**, and pre-reaction clusters **2a**−**d**). Figure S1 (relative energies, selected geometrical characteristics and stereochemical assignment of eight lowest-energy transition structures optimized at the B3LYP/6-31G(d,p) level of theory). Figure S2 (*syn*-(2*R*,3*R*,4*S*)-TS-3a, optimized at B3LYP/6-31G(d,p) and the selected points A−C along the reaction coordinate for the epoxidation of conformer 1b after the barrier has been crossed, were determined by Intrinsic-Reaction-Coordinate (IRC) analysis (B3LYP/6-31G(d)). Beyond the *syn*-(*2R,3R,4S*)-TS-3a transition state, analysis of the intrinsic reaction coordinate suggests that the net chemical event is the formal transfer of HO^+ to the carbon−carbon double bond). This material is available free of charge via the Internet at http://pubs.acs.org.

JO0009548